Interaction and Multiscale Mechanics, Vol. 3, No. 3 (2010) 277-298
DOI: http://dx.doi.org/10.12989/imm.2010.3.3.277

The coupling of complex variable-reproducing kernel particle method and finite element method for two-dimensional potential problems

Li Chen[1,2], K.M. Liew[1]* and Yumin Cheng[3]

[1]*Department of Building and Construction, City University of Hong Kong, Tat Chee Avenue, Kowloon, Hong Kong SAR*
[2]*Department of Engineering Mechanics, Chang'an University, Xi'an 710064, China*
[3]*Shanghai Institute of Applied Mathematics and Mechanics, Shanghai University, Shanghai 200072, China*

(Received July 7, 2010, Accepted September 21, 2010)

Abstract. The complex variable reproducing kernel particle method (CVRKPM) and the FEM are coupled in this paper to analyze the two-dimensional potential problems. The coupled method not only conveniently imposes the essential boundary conditions, but also exploits the advantages of the individual methods while avoiding their disadvantages, resulting in improved computational efficiency. A hybrid approximation function is applied to combine the CVRKPM with the FEM. Formulations of the coupled method are presented in detail. Three numerical examples of the two-dimensional potential problems are presented to demonstrate the effectiveness of the new method.

Keywords: potential; complex variable reproducing kernel particle method; finite element method; coupled CVRKP-FE method; hybrid approximation function.

1. Introduction

Partial differential equations arise in connection with various physical and geometrical problems in which the functions involved depend on two or more independent variables, usually on time t and on one or several space variables. The potential problem is one of the most important partial differential equations in engineering mathematics, because it occurs in connection with gravitational fields, electrostatics fields, steady-state heat conduction, incompressible fluid flow, and many other areas (Selvadurai 2000). Mathematically, the problem is a function that satisfies a given partial differential equation and particular boundary conditions. In physical term, this problem is independent of time and involves only the space coordinates, as in Poisson's equation or the Laplace equation with Dirichlet, Neuman, or mixed conditions. Due to the complex material properties, boundary conditions, boundary shapes, etc., analytical solutions are usually difficult to obtain except for problems with simple geometry and boundary conditions. As a result, various numerical models are usually required. It is noted that numerical methods such as the finite element

* Corresponding author, Chair Professor, E-mail: kmliew@cityu.edu.hk

method (FEM) has been well established over the past a few decades and has been successfully applied to potential problems. However, it also has limit, the spatial domain where the partial differential governing equations are defined is often discretized into meshes. In the general, the creation of suitable meshes is very essential for acquiring accurate results. However, mesh generation process consumes a lot of time and labor for some problems especially for discontinuous and high gradient problems.

To avoid the disadvantages of FEM, meshless methods, which only require a set of nodes scattered within the problem domain to constructed the approximate functions and easy to prepare initial date, have developed rapidly as new computational techniques in structural mechanics and engineering analysis (Belytschko *et al*. 1996). Meshless methods have some advantages in solving certain science and engineering problems that are not well suited to the use of traditional computational methods, especially for problems of extremely large deformation, dynamic fracturing, and explosion (Liew *et al*. 2002a, Liew *et al*. 2002b). Those meshless methods that have been developed include the element-free Galerkin (EFG) method (Belytschko *et al*. 1994), the reproducing kernel particle (RKP) method (Liu *et al*. 1995), the the radial basis function (RBF) (Liu *et al*. 2005), the finite point method (FPM) (Onarte 1996), the meshless local Petrov-Galerkin (MLPG) method (Atluri and Zhu 1998), the meshless point collocation method (PCM) (Aluru 2000), the radial point interpolation method (Liew and Chen 2004a, Liew and Chen 2004b), the moving least-squares differential quadrature meshfree method (Liew *et al*. 2003, Liew and Huang 2003, Liew *et al*. (2004), the wavelet particle method (WPM) (Liu and Chen 1995), the mesh-free kp-Ritz method (Zhao *et al*. 2004, Zhao *et al*. 2007, Liew *et al*. 2004), the complex variable meshless method (Liew *et al*. 2007, Liew and Cheng 2009), and the meshless methods with boundary integral equations (Zhu *et al*. 1998, Sun *et al*. 2006, Kothnur *et al*. 1999, Liew *et al*. 2005, Liew *et al*. 2006).

The RKPM was originally introduced to improve the accuracy of the smoothed particle hydrodynamics method (SPH) (Liu *et al*. 1995), which was the earliest meshless method. In the RKPM, the kernel function is modified by introducing a correction function to satisfy the reproducing conditions, so the resulting modified kernel function reproduces polynomials exactly to a specific order and fulfills the completeness requirement. The RKPM not only shares the features of all meshless methods but also has some unique features, such as time or space localization, hp-like adaptivity, and multiresolution analysis (Liu *et al*. 1996). All of these make the RKPM a novel approach for structural dynamics (Liu *et al*. 1995, Liew *et al*. 2002), large deformation problems (Chen *et al*. 1996, Liu and Jun 1998), and fluid mechanics (Liu *et al*. 1997).

Although the RKPM has many advantages compared with other numerical methods, it has a great computational cost because of the large number of nodes selected in the domain of the problem. Hence, the complex variable reproducing kernel particle method (CVRKPM) was developed on the basis of the RKPM, and was then applied to two-dimensional elasticity and transient heat conduction problems (Chen and Cheng 2008a, Chen and Cheng 2008b). The advantages of the CVRKPM are that the correction function of a 2-D problem is formed with a 1-D basis function when the shape function is formed. As the unknown coefficients of the correction function in the complex variable reproducing kernel particle approximation are fewer than in the reproducing kernel particle approximation, we need fewer nodes with domains of influence that cover an arbitrary point in the domain, and thus require fewer nodes in the whole domain. Hence, under the same quantity of nodes used to discretize the problem domain, the CVRKPM is more precise than the RKPM.

Although the CVRKPM has some advantages, it still presents technical difficulties. The two most important difficulties are:

(1) The shape functions of the CVRKPM lack the Kronecker delta function property, which makes it difficult to impose the essential boundary conditions of the problem.

(2) When compared with the traditional FEM, the CVRKPM has a higher computational cost for the construction of shape functions and also for the formation of a global equation system. This makes the CVRKPM too expensive for problems requiring a dense distribution of points over a large domain area.

It is often desirable and beneficial to combine two established numerical methods to exploit their advantages while avoiding their disadvantages. In this paper, the CVRKPM and the FEM are combined as the CVRKP-FE method for analyzing the two-dimensional (2D) potential problems. The coupled CVRKP-FE method is promising as it reduces the computational time of the CVRKPM and simplifies the imposition of the essential boundary conditions. This coupled method employs interface elements, within which the shape functions are comprised of CVRKPM and FEM shape functions. Both the FE interpolations and the CVRKP approximation satisfy consistency, which means that the modified interface shape functions satisfy consistency, thus ensuring convergence of the method. The formulations of the CVRKP-FE method are given together with some numerical examples to demonstrate the applicability of the present method.

2. Combination techniques

Consider a two-dimensional potential problem. The problem domain consists of two sub-domains, Ω_1 and Ω_2, joined by an interface boundary, Γ_I. Numerical method 1 is used in Ω_1 and numerical method 2 is used in Ω_2, as shown in Fig. 1. In the coupling method, the field variable compatibility and the force equilibrium conditions on Γ_I must be satisfied (Gu and Liu 2005). Thus,

1) The nodal variables $u_I^{(1)}$ and $u_I^{(2)}$ at Γ_I for Ω_1 and Ω_2 should be equal, i.e.

$$u_I^{(1)} = u_I^{(2)} = u_I \tag{1}$$

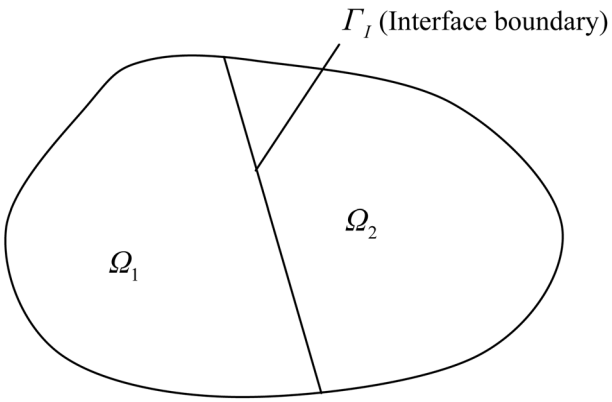

Fig. 1 Two sub-domains and the interface boundary in the coupled method

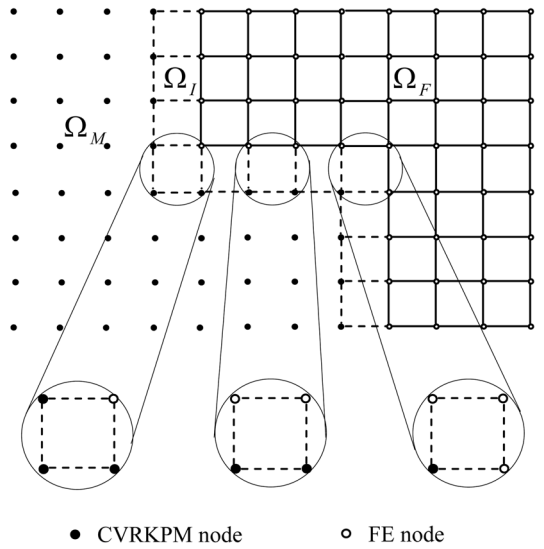

Fig. 2 Sub-domains used for FE-CVRKP coupling

2) The summation of forces $\Gamma_I^{(1)}$ and $\Gamma_I^{(2)}$ at Γ_I for Ω_1 and Ω_2 should be zero, i.e.

$$F_I^{(1)} = F_I^{(2)} = 0 \tag{2}$$

If shape functions along the interface boundary Γ_I in both domain Ω_1 and domain Ω_2 satisfy the Kronecker delta function properties, these two numerical methods can be combined directly along that boundary. However, because the CVRKP shape functions lack the delta function property, u^h in the CVRKP approximation differs from the nodal variable value u at point $\boldsymbol{x}$. It is thus impossible to couple the CVRKPM and the FEM directly along Γ_I. Techniques are needed to satisfy the combination conditions in Eqs. (1) and (2). Among these techniques, the hybrid approximation function is the more widely used (Belytschko and Organ 1995).

3. Using hybrid field variable approximation

The coupling between the FEM and the CVRKPM is accomplished by introducing interface elements between the FEM and CVRKPM domains. A detailed illustration of the interface domain is shown in Fig. 2. Ω_I is a layer of sub-domain along interface boundary Γ_I within the meshless domain Ω_M. Ω_I is the interface domain and it is divided into several interface elements (finite elements). In these interface elements, a hybrid field variable approximation is defined to satisfy field variable continuity across the interface boundaries. Before these interface elements are described in detail, the separate FE and CVRKP field variable approximations will be defined.

3.1 FE field variable interpolation function

The standard FE interpolation function for the field variable u in an isoparametric element is

$$u^F(\boldsymbol{x}) = \sum_{I=1}^{n_F} N_I(\boldsymbol{\zeta}(\boldsymbol{x})) \cdot u_I \qquad \boldsymbol{x} \in \Omega_F^e \tag{3}$$

where n_F is the number of element nodes. For example, if the 4-node element used here, N_I are the standard bilinear shape functions

$$N_I(\boldsymbol{\zeta}(\boldsymbol{x})) = \frac{1}{4}(1 + \xi_I \xi(\boldsymbol{x})) \cdot (1 + \eta_I \eta(\boldsymbol{x})) \tag{4}$$

In the above expressions, $\boldsymbol{\zeta}(\boldsymbol{x}) = (\xi(\boldsymbol{x}), \eta(\boldsymbol{x}))$ is a mapping from the physical domain to the parent domain (only the inverse mapping is usually defined), and (ξ_I, η_I) are the nodal coordinates in the parent domain ($\xi \in [-1, 1]$, $\eta \in [-1, 1]$).

3.2 CVRKPM field variable approximation

Similar to the reproducing kernel particle methods, complex variable reproducing kernel particle approximation is a class of operators that reproduces the function itself through integration over the entire domain (Liu *et al.* 1995). Consider a random function $\bar{u}(z)$ that is defined in the problem domain Ω with the boundary Γ. The reproducing kernel approximation of function $\bar{u}(z)$ at point z, denoted $\bar{u}^h(z)$, is given by

$$\bar{u}^h(z) = u_1^h(z) + i u_2^h(z) = \int_\Omega \bar{u}(z') \cdot \bar{w}_h(z - z') \cdot dz', \qquad (z = x_1 + i x_2 \in \Omega) \tag{5}$$

Suppose that the domain Ω is discretized by a set of nodes $(z_1, z_2, \ldots, z_{n_t})$, where z_I is the location of node I and n_t is the total number of nodes in the whole domain. It is assumed that only the nodes surrounding one point z have an effect on $\bar{u}(z)$. The sub-domain that encompasses these surrounding nodes is called the support domain of point z. By the use of a simple trapezoidal rule, the estimated value of $\bar{u}(z)$ can be obtained through the following weighted linear combination

$$\bar{u}^h(z) = \sum_{I=1}^{n} \bar{u}(z_I) \cdot \bar{w}_h(z - z_I) \cdot \Delta V_I = \sum_{I=1}^{n} C(z; z - z_I) \cdot w_h(z - z_I) \cdot \Delta V_I \cdot \bar{u}(z_I) \tag{6}$$

where n is the total number of nodes in the support domain of point z, $\bar{w}_h(z - z')$ is the weight function which has a compact support domain, ΔV_I is the volume of node I and represents the integration weight, and $C(z; z - z')$ is the correction function. In this study, the cubic spline function is chosen as the weight function. The correction function $C(z; z - z')$ is expressed as a linear combination of polynomial basis functions

$$C(z; z - z') = \sum_{i=0}^{N} p_i(z - z') \cdot b_i(z) = \boldsymbol{p}^{\mathrm{T}}(z - z')\boldsymbol{b}(z) \tag{7}$$

where N is the highest order of polynomial basis functions, $p_i(z - z')$ are the basis functions, and $b_i(z)$ are the corresponding coefficients, which are obtained via the reproducing conditions as follows

$$\boldsymbol{M}(z)\boldsymbol{b}(z) = \begin{pmatrix} \bar{m}_0(z) \\ \bar{m}_1(z) \\ \vdots \\ \bar{m}_N(z) \end{pmatrix} = \begin{pmatrix} 1 \\ 0 \\ \vdots \\ 0 \end{pmatrix} \tag{8}$$

in which

$$\boldsymbol{M}(z) = \begin{bmatrix} m_0(z) & m_1(z) & \cdots & m_N(z) \\ m_1(z) & m_2(z) & \cdots & m_{N+1}(z) \\ \vdots & \vdots & \ddots & \vdots \\ m_N(z) & m_{N+1}(z) & \cdots & m_{2N}(z) \end{bmatrix}$$

$$= \sum_{I=1}^{n} \boldsymbol{p}(z-z_I) \cdot \boldsymbol{p}^{\mathrm{T}}(z-z_I) \cdot w_h(z-z_I) \cdot \Delta V_I \tag{9}$$

Let

$$\boldsymbol{H} = (1, 0, \ldots, 0)^T \tag{10}$$

The corresponding compact matrix form

$$\boldsymbol{M}(z) \cdot \boldsymbol{b}(z) = \boldsymbol{H} \tag{11}$$

From Eq. (11), we have

$$\boldsymbol{b}(z) = \boldsymbol{M}^{-1}(z) \cdot \boldsymbol{H} \tag{12}$$

From Eq. (6), the expression of the trial function $\bar{u}^h(z)$ can be written as

$$\bar{u}^h(z) = \boldsymbol{\Phi}(z)\bar{\boldsymbol{u}} = \sum_{I=1}^{n} \Phi_I(z)\bar{u}(z_I) \tag{13}$$

Therefore, we have

$$u_1^h(z) = \mathrm{Re}[\boldsymbol{\Phi}(z)\bar{\boldsymbol{u}}] = \mathrm{Re}\left[\sum_{I=1}^{n} \Phi_I(z)\bar{u}(z_I)\right] \tag{14}$$

$$u_2^h(z) = \mathrm{Im}[\boldsymbol{\Phi}(z)\bar{\boldsymbol{u}}] = \mathrm{Im}\left[\sum_{I=1}^{n} \Phi_I(z)\bar{u}(z_I)\right] \tag{15}$$

where $\boldsymbol{\Phi}(z)$ is defined as the shape function of the CVRKPM, and

$$\boldsymbol{\Phi}(z) = (\Phi_1(z), \Phi_2(z), \ldots, \Phi_n(z)) \tag{16}$$

$$\Phi_I(z) = C(z;z-z_I)w_h(z-z_I)\Delta V_I \tag{17}$$

Because the field variable u of potential problems is scalar, the CVRKP approximations are defined in a form similar to Eq. (3)

$$u^M(z) = u_1^h(z) = \mathrm{Re}[\boldsymbol{\Phi}(z)\boldsymbol{u}] = \tilde{\boldsymbol{\Phi}}(z)\boldsymbol{u} \tag{18}$$

and

$$\mathrm{Im}[\boldsymbol{\Phi}(z)\boldsymbol{u}] = \sum_{I=1}^{n} \mathrm{Im}[\Phi_I(z)] \cdot u(z_I) = 0 \tag{19}$$

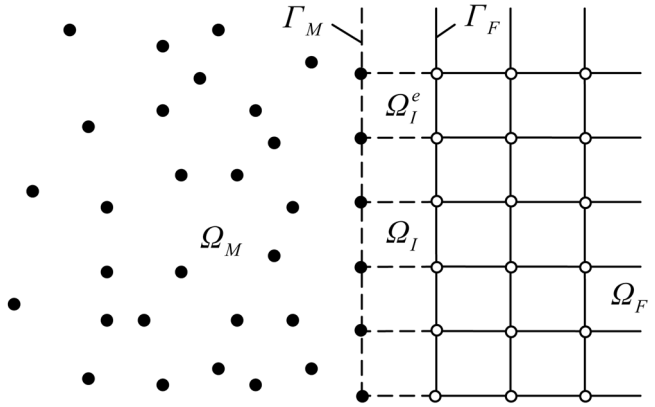

Fig. 3 Interface element used for FE-CVRKP coupling

where

$$\tilde{\Phi}(z) = (\tilde{\Phi}_1(z), \tilde{\Phi}_2(z), \ldots, \tilde{\Phi}_n(z)) \tag{20}$$

$$\Phi_I(z) = \mathrm{Re}[\Phi_I(z)] \tag{21}$$

3.3 Interface field variable approximation

To illustrate the coupling procedure, again consider the domain in Fig. 2 along with the additional detail shown in Fig. 3. In Ω_M, the potential u at a point is approximated using the CVRKP approximants in (18), and in Ω_F, the finite element interpolants in (3) are employed in each element Ω_F^e. In Ω_I, the interface region, the following expression is used (Belytschko and Organ 1995, Dolbow and Belytschko 1999)

$$u^h(\boldsymbol{x}) = \begin{cases} \beta(\boldsymbol{x}) \cdot u^M(z(\boldsymbol{x})) + [1 - \beta(\boldsymbol{x})] u^F(\zeta(\boldsymbol{x})) & \boldsymbol{x} \in \Omega_I \\ u^M(z(\boldsymbol{x})) & \boldsymbol{x} \in \Omega_M - \Omega_I \end{cases} \tag{22}$$

where $u^h(\boldsymbol{x})$ is the potential approximation of a point in Ω_I, u^M and u^F are approximations for $u(\boldsymbol{x})$ in Ω_I given by the FE and CVRKP approximations, respectively, and $\beta(\boldsymbol{x})$ is a blending function that is constructed with the use of a linear ramp function $R(\boldsymbol{x})$. $R(\boldsymbol{x})$ is defined using the finite element shape functions (Belytschko and Organ 1995), i.e.

$$R(\boldsymbol{x}) = \sum_{i=1}^{k} N_i(\boldsymbol{x}) \qquad \boldsymbol{x}_i \in \Gamma_M \tag{23}$$

where k is the number of nodes located on the meshless boundary Γ_M for an interface element. In other words, the linear ramp function is equal to the sum of the FE shape functions that are associated with the interface element nodes on the meshless boundary Γ_M. According to the property of the FE shape function, $R(\boldsymbol{x})$ will be unity on meshless boundary Γ_M and vanish on boundary Γ_F (Γ_I), i.e.

$$R(\boldsymbol{x}) = \begin{cases} 0 & \boldsymbol{x} \in \Gamma_F \\ 1 & \boldsymbol{x} \in \Gamma_M \end{cases} \tag{24}$$

The smooth blending function and its derivatives are given by

$$\beta(\boldsymbol{x}) = 3R^2(\boldsymbol{x}) - 2R^3(\boldsymbol{x}) \tag{25}$$

Note that

$$\beta(\boldsymbol{x}) = \begin{cases} 0 & \boldsymbol{x} \in \Gamma_F \\ 1 & \boldsymbol{x} \in \Gamma_M \end{cases} \tag{26}$$

hence, the approximation (22) reduces to u^M (18) on Γ_M and u^F (3) on Γ_F, thus ensuring the continuity. At the same time, it also provides for continuous derivatives along the meshless boundary Γ_M.

The interface shape functions can be developed by substituting the potential approximations (18) and (3) into (22), i.e.

$$u^h(\boldsymbol{x}) = \beta(\boldsymbol{x}) \cdot \sum_{I=1}^{n} \tilde{\Phi}_I(z(\boldsymbol{x})) \cdot u_I + [1 - \beta(\boldsymbol{x})] \cdot \sum_{I=1}^{n_F} N_I(\zeta(\boldsymbol{x})) \cdot u_I = \sum_{I=1}^{n} \overline{\Phi}_I(\boldsymbol{x}) \cdot u_I$$

$$\boldsymbol{x} \in \Omega_I^e \tag{27}$$

where the hybrid shape functions of the interface element are

$$\overline{\Phi}_I(\boldsymbol{x}) = \begin{cases} \beta(\boldsymbol{x}) \cdot \tilde{\Phi}_I(z) + [1 - \beta(\boldsymbol{x})] N_I(\zeta(\boldsymbol{x})) & \boldsymbol{x}_I \in \Omega_I^e \quad \text{(28a)} \\ \beta(\boldsymbol{x}) \cdot \tilde{\Phi}_I(z) & \boldsymbol{x}_I \notin \Omega_I^e \quad \text{(28b)} \end{cases}$$

Eq. (28a) applies to the shape functions associated with the interface element nodes and Eq. (28b) applies to those associated with nodes outside the particular interface element.

The derivatives of the interface shape function are

$$\overline{\Phi}_{I,j}(\boldsymbol{x}) = \begin{cases} \beta(\boldsymbol{x})\tilde{\Phi}_{I,j} + \beta_{,j}\tilde{\Phi}_I + [1 - \beta(\boldsymbol{x})]N_{I,j} - \beta_{,j} N_I & \boldsymbol{x}_I \in \Omega_I^e \\ \beta(\boldsymbol{x})\tilde{\Phi}_{I,j} + \beta_{,j}\tilde{\Phi}_I & \boldsymbol{x}_I \notin \Omega_I^e \end{cases} \tag{29}$$

where

$$\beta_{,j}(\boldsymbol{x}) = [6R(\boldsymbol{x}) - 6R^2(\boldsymbol{x})]R_{,j} \tag{30}$$

in which

$$R_{,j}(\boldsymbol{x}) = \sum_{I=1}^{k} N_{I,j}(\boldsymbol{x}) \qquad \boldsymbol{x}_I \in \Gamma_M \tag{31}$$

This provides for continuous derivatives along the meshless boundary Γ_M.

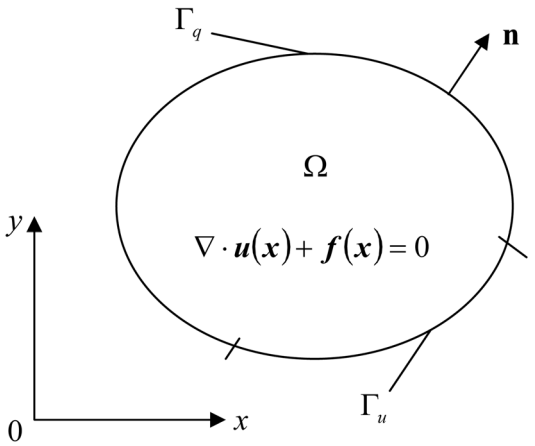

Fig. 4 Two-dimensional potential problem

4. CVRKP-FE method for 2D potential problems

4.1 2D Potential Formulations

Consider a Poisson's equation for a problem governing the potential u in a 2D domain Ω bounded by contour Γ (see Fig. 4)

$$\nabla \cdot \boldsymbol{u}(\boldsymbol{x}) + Q(\boldsymbol{x}) = 0, \text{ in } \Omega \tag{32}$$

where $Q(\boldsymbol{x})$ is a given source function of x and y, and Ω is the domain of the body. In the general case, boundary Γ can have mixed boundary conditions. On one part of boundary Γ_u, the potential u is prescribed, and on the remaining part, Γ_q, the secondary variables, flux ($q = \partial u / \partial n$), are prescribed, i.e.

$$\boldsymbol{u}(\boldsymbol{x}) = \bar{\boldsymbol{u}}(\boldsymbol{x}), \qquad \boldsymbol{x} \in \Gamma_u \tag{33}$$

$$q(\boldsymbol{x}) = \frac{\partial u(\boldsymbol{x})}{\partial n} = \bar{q}(\boldsymbol{x}) \qquad \boldsymbol{x} \in \Gamma_q \tag{34}$$

where the boundary $\Gamma = \partial\Omega = \Gamma_u + \Gamma_q$, and $\boldsymbol{n}$ is the unit outward normal to the boundary. For example, in a steady-state heat transfer problem, which is a tropical Poisson's problem, u is the temperature, q is the heat flux function, and $Q(\boldsymbol{x})$ is internal heat generation.

One of the aims for coupling the CVRKPM and FEM is to simplify the imposition of the essential boundary conditions, so the essential boundary should be included in the FEM domain. As both the FEM and the CVRKPM are discretized by the Galerkin approximations, the weak forms can be used directly in the coupled method without any modifications. The Galerkin weak form is

$$\int_\Omega \delta(\boldsymbol{L}u)^{\mathrm{T}} \cdot (\boldsymbol{L}u)\mathrm{d}\Omega - \int_\Omega \delta u \cdot Q\mathrm{d}\Omega - \int_{\Gamma_q} \delta u \cdot \bar{q}\mathrm{d}\Gamma = 0 \tag{35}$$

where

$$\boldsymbol{L}(\cdot) = \begin{bmatrix} \dfrac{\partial}{\partial x_1} \\ \dfrac{\partial}{\partial x_2} \end{bmatrix} (\cdot) \tag{36}$$

The weak form in Eq. (35) is used in the Galerkin procedure to develop the discrete equations. In the weak form, approximate u and $\boldsymbol{L}u$ by

$$u^h(\boldsymbol{x}) = \sum_{I=1}^{n} \hat{\Phi}_I(\boldsymbol{x}) \cdot u_I = \hat{\boldsymbol{\Phi}}_I(\boldsymbol{x}) \cdot \boldsymbol{u} \tag{37}$$

$$\boldsymbol{L}u^h = \hat{\boldsymbol{B}}(\boldsymbol{x}) \cdot \boldsymbol{u} \tag{38}$$

where

$$\hat{\boldsymbol{\Phi}} = (\hat{\Phi}_1(\boldsymbol{x}), \hat{\Phi}_2(\boldsymbol{x}), \ldots, \hat{\Phi}_n(\boldsymbol{x})) \tag{39}$$

$$\hat{\Phi}_I(\boldsymbol{x}) = \begin{cases} N_I(\zeta(\boldsymbol{x})) & \boldsymbol{x} \in \Omega_F \\ \tilde{\Phi}_I(z(\boldsymbol{x})) & \boldsymbol{x} \in \Omega_M - \Omega_I \\ \overline{\Phi}_I(\boldsymbol{x}) & \boldsymbol{x} \in \Omega_I^e \end{cases} \tag{40}$$

and

$$\hat{\boldsymbol{B}} = (\hat{\boldsymbol{B}}_1(\boldsymbol{x}), \hat{\boldsymbol{B}}_2(\boldsymbol{x}), \ldots, \hat{\boldsymbol{B}}_n(\boldsymbol{x})) \tag{41}$$

$$\hat{\boldsymbol{B}}_I(\boldsymbol{x}) = \begin{cases} \boldsymbol{B}_I^F(\zeta(\boldsymbol{x})) & \boldsymbol{x} \in \Omega_F \\ \boldsymbol{B}_I^M(z(\boldsymbol{x})) & \boldsymbol{x} \in \Omega_M - \Omega_I \\ \boldsymbol{B}_I^I(\boldsymbol{x}) & \boldsymbol{x} \in \Omega_I^e \end{cases} \tag{42}$$

in which

$$\boldsymbol{B}_I^F(\boldsymbol{x}) = \begin{bmatrix} N_{I,x}(\xi(\boldsymbol{x})) \\ N_{I,y}(\xi(\boldsymbol{x})) \end{bmatrix} \tag{43}$$

$$\boldsymbol{B}_I^M(z) = \begin{bmatrix} \mathrm{Re}[\Phi_{i,x}(z)] \\ \mathrm{Re}[\Phi_{i,y}(z)] \end{bmatrix} \tag{44}$$

$$\boldsymbol{B}_I^I(\boldsymbol{x}) = \begin{bmatrix} \overline{\Phi}_{I,x}(\boldsymbol{x}) \\ \overline{\Phi}_{I,y}(\boldsymbol{x}) \end{bmatrix} \tag{45}$$

Substituting Eq. (37) and Eq. (38) into Eq. (35), we have

$$\int_{\Omega} \delta(\hat{\boldsymbol{B}} \cdot u)^{\mathrm{T}} \cdot (\hat{\boldsymbol{B}} \cdot u) \mathrm{d}\Omega - \int_{\Omega} \delta(\hat{\boldsymbol{\Phi}} \cdot \boldsymbol{u}) \cdot Q \mathrm{d}\Omega - \int_{\Gamma_q} \delta(\hat{\boldsymbol{\Phi}} \cdot \boldsymbol{u}) \cdot \bar{q} \mathrm{d}\Gamma = 0 \tag{46}$$

The nodal test function values $\delta \boldsymbol{u}^{\mathrm{T}}$ are arbitrary, resulting in

$$\boldsymbol{K}\boldsymbol{u} = \boldsymbol{F} \tag{47}$$

where

$$K_{IJ} = \int_{\Omega} \hat{\boldsymbol{B}}_I^{\mathrm{T}} \cdot \hat{\boldsymbol{B}}_J \mathrm{d}\Omega \tag{48}$$

$$f_I = \int_{\Omega} \hat{\Phi}_I(\boldsymbol{x}) \cdot Q \mathrm{d}\Omega + \int_{\Gamma_q} \hat{\Phi}_I(\boldsymbol{x}) \cdot \bar{q} \mathrm{d}\Gamma \tag{49}$$

5. Numerical experiments

In this section, numerical results for selected example problems are presented to illustrate the applicability of the present CVRKP-FE method.

5.1 Convergence analysis and error estimation

The convergence study of the proposed method on the 2D potential problems is carried out by analyzing the final potential function values under different discretization schemes and different scaling factors $d_{\max}$ for the nodes of the study field.

For the purpose of error estimation and convergence studies, the Sobolev norms $\| \|_k$ are calculated. In the following numerical examples, the Sobolev norms for $k = 0$ and $k = 1$ are considered for the present potential problem. These norms are defined as

$$\|u\|_0 = \left(\int_{\Omega} u^2 \mathrm{d}\Omega \right)^{\frac{1}{2}} \tag{50}$$

and

$$\|u\|_1 = \left(\int_{\Omega} u^2 + (|\nabla u|)^2 \mathrm{d}\Omega \right)^{\frac{1}{2}} \tag{51}$$

The relative errors are defined as

$$r_k = \frac{\left\| u^{\mathrm{num}} - u^{\mathrm{exact}} \right\|_k}{\left\| u^{\mathrm{exact}} \right\|_k} \qquad k = 0, 1 \tag{52}$$

We apply the present method on the 2D Poisson's equation with Dirichlet boundary conditions on a rectangular domain. The governing equation and the boundary conditions are

$$\frac{\partial^2 u}{\partial x_1^2} + \frac{\partial^2 u}{\partial x_2^2} - 4 = 0, \quad x_1 \in [0, 8], \quad x_2 \in [-3, 3] \tag{53}$$

$$u(0, x_2) = x_2^2 \qquad -3 < x_2 < 3 \tag{54}$$

$$u(8, x_2) = 64 + x_2^2 \qquad -3 < x_2 < 3 \tag{55}$$

$$u(x_1, 3) = x_1^2 + 9 \qquad 0 < x_1 < 8 \tag{56}$$

and

$$u(x_1, -3) = x_1^2 + 9 \qquad 0 < x_1 < 8 \tag{57}$$

The analytical solution of this problem is

$$u(x_1, x_2) = x_1^2 + x_2^2 \tag{58}$$

It is known that the choice of scaling factors $d_{\max}$ has influence on the support domain of nodes within the meshless domain Ω_M, and further influence the performance of the present coupled method. Therefore, the influences of scaling factors $d_{\max}$ on the numerical results are studied firstly, where different regular nodal distributions are used. The relation of between the relative error norm values and scaling factors $d_{\max}$ is plotted in Fig. 5. From the numerical result, we observed that it is a good choice to take $d_{\max} = 1.3$. With the above analysis, $d_{\max} = 1.3$ is taken in the following examples. Moreover, the relative error norm values decrease with the increase of number of nodes under certain $d_{\max}$.

Regular nodes distribution of $399(21 \times 19)$, $255(17 \times 15)$ and $63(9 \times 7)$ are used to study the convergence of the present coupled method. The size h in the figure is defined as the distance in x_1 direction between two neighboring nodes with the same the x_2 coordinate. The relative errors and the convergence rates for norms $\|\ \|_0$ and $\|\ \|_1$ for the present coupled method, the CVRKP method and the FEM with mesh refinement are shown in Fig. 6 and in Fig. 7, respectively. From these two figures, it can be seen that the present method has high rates of convergence for norms $\|\ \|_0$ and $\|\ \|_1$, and gives reasonably accurate results for the unknown variable and its derivatives. It can be also observed the convergence rates for both the present coupled method and the MLPG method are almost similar if the best scaling factors $d_{\max}$ are used, and the present coupled method has the

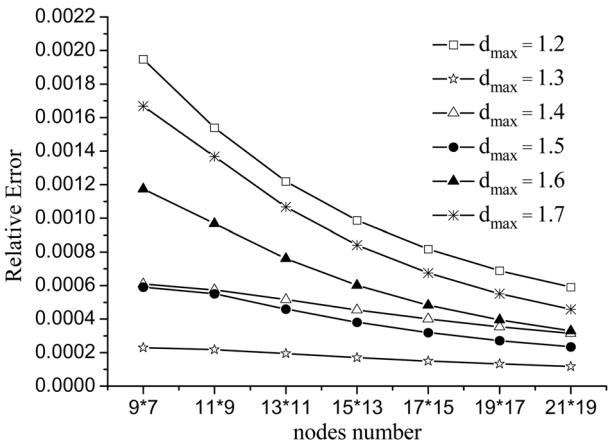

Fig. 5 Influence of different parameter $d_{\max}$ on the relative error

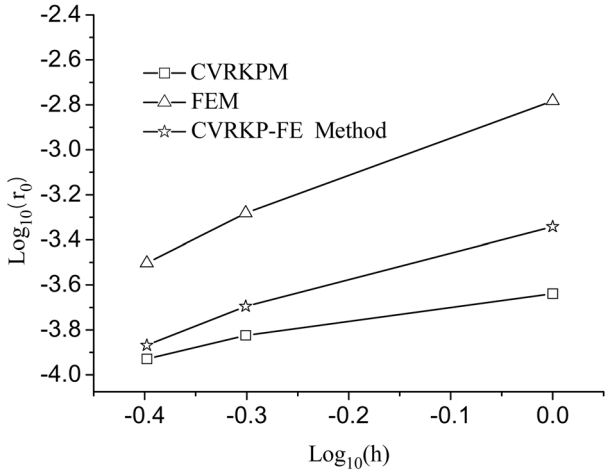

Fig. 6 Relative errors and convergence rates for norm $\|\ \|_0$

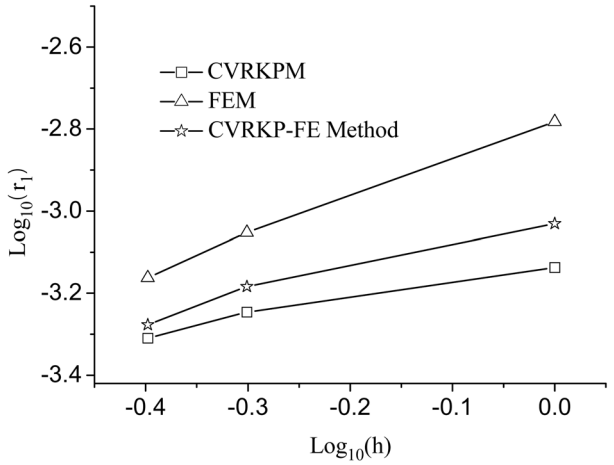

Fig. 7 Relative errors and convergence rates for norm $\|\ \|_1$

better convergence than the FEM.

Fig. 8 shows the analytical solution and the numerical solution under different number of nodes with $d_{\max} = 1.3$. It is observed that the results obtained by the present coupled method agree well with the analytical solution even fewer nodes are used.

Figs. 9 and 10 plot the analytical solution and numerical solutions using the present coupled method, CVRKP method and FEM along x_2 and x_1 axes, respectively. It can be observed that the proposed coupled method takes less computation time compared with the CVRKP method.

5.2. Numerical studies

Three example problems are presented to demonstrate the applicability of the CVRKP-FE method

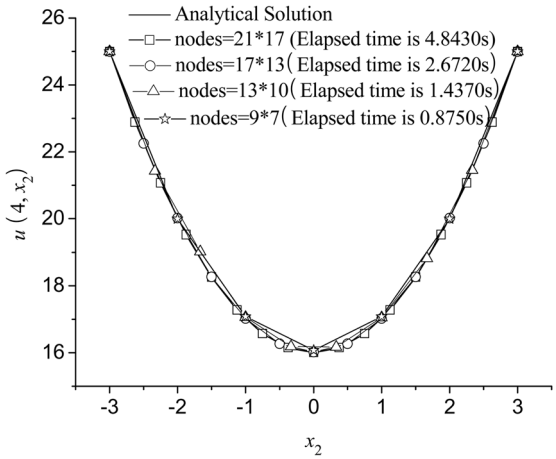

Fig. 8 Results obtained by the CVRKP-FE method with different number of nodes

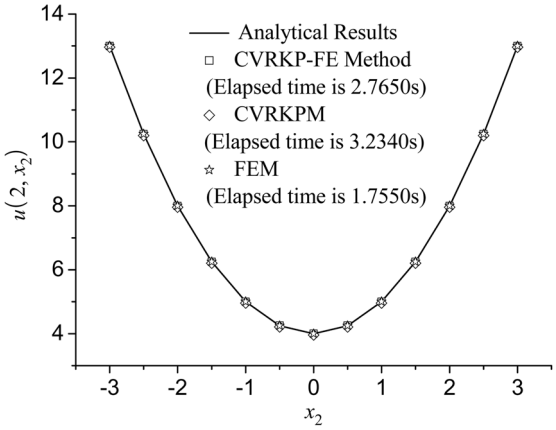

Fig. 9 Comparison of the potential distributions at $x_1 = 2$ along x_2 coordinate

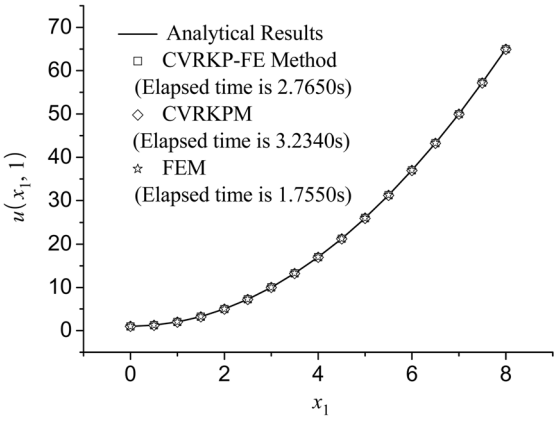

Fig. 10 Comparison of the potential distributions at $x_2 = 1$ along x_1 coordinate

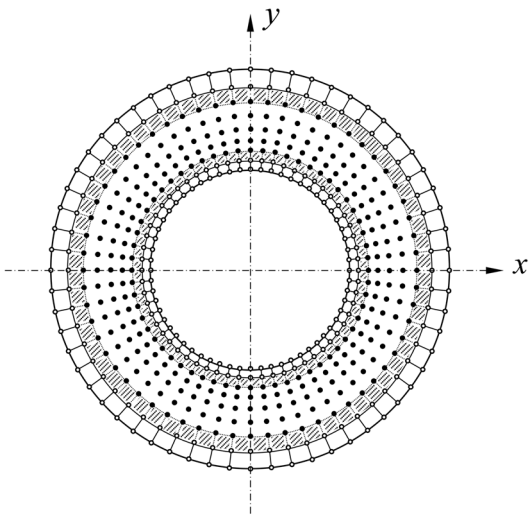

Fig. 11 Node and mesh arrangement on a torus domain. The shaded elements are those adjacent to the interface of the FE domain (outside) and the CVRKPM domain (inside)

for two-dimensional potential problems. The results that are obtained for these examples are compared with the CVRKPM and existing analytical solutions that have been published in the literature.

In the numerical examples presented in this section, a regular or irregular arrangement of nodes and the background mesh of cells are used for the numerical integrations to calculate the system equation. A 4×4 Gaussian quadrature over the elements is used for integration. The linear basis and cubic spline weight function are used in the CVRKP approximation. In addition, based on the results of the previous numerical examples, we take the $d_{\max} = 1.3$.

5.2.1 Poisson's equation with Dirichlet problems on a torus

The first example considered is a 2D Poisson equation with Dirichlet boundary conditions on the torus, as shown in Fig. 11. The Poisson equation is

$$\frac{\partial^2 u}{\partial x_1^2} + \frac{\partial^2 u}{\partial x_2^2} - 4 = 0, \quad a < r < b, \quad 0 < \theta < 2\pi \tag{59}$$

with the boundary conditions

$$u(a, \theta) = 0 \tag{60}$$

$$u(b, \theta) = 0 \tag{61}$$

The analytical solution of this problem is

$$u(r, \theta) = (r^2 - a^2) - (b^2 - a^2)\left(\frac{\log r - \log a}{\log b - \log a}\right) \tag{62}$$

The following parameters are used for the numerical simulation: $a = 1$ and $b = 1$. Fig. 11 shows the finite element mesh and the distributions of particles. The nodes are arranged regularly in

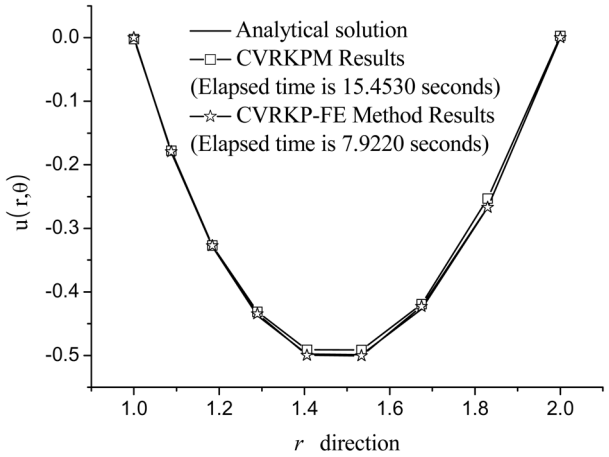

Fig. 12 Results obtained with the analytical, CVRKPM and CVRKPM-FEM solutions along the r direction at any angle

the θ direction and irregularly in the r direction.

The analytical and numerical solutions using both the CVRKPM and CVRKP-FE method along the r axis at any angle are plotted in Fig. 12. The results of the CVRKP-FE method agree well with the analytical solution. However, the CVRKP-FE method takes around half the time to calculate than those of the CVRKPM.

5.2.2 Laplace equation with mixed boundary conditions on a cube

The second example considered is a 2D Laplace equation with mixed boundary conditions. Supposing a steady temperature field on a rectangular domain, the governing equation is

$$\nabla^2 T = \frac{\partial^2 T}{\partial x_1^2} + \frac{\partial^2 T}{\partial x_2^2} = 0, \qquad x_1 \in [0, 5], x_2 \in [0, 10] \tag{63}$$

with the boundary conditions

$$T(x_1, 0) = 0 \qquad 0 < x_1 < 5 \tag{64}$$

$$T(0, x_2) = 0 \qquad 0 < x_2 < 10 \tag{65}$$

$$T(x_1, 10) = 100\sin(\pi x_1 / 10) \qquad 0 < x_1 < 5 \tag{66}$$

and

$$\frac{\partial T(5, x_2)}{\partial x_1} = 0 \qquad 0 < x_2 < 10 \tag{67}$$

The analytical solution of this temperature field is

$$u(x_1, x_2) = \frac{100\sin(\pi x_1 / 10)\sinh(\pi x_2 / 10)}{\sinh(\pi)} \tag{68}$$

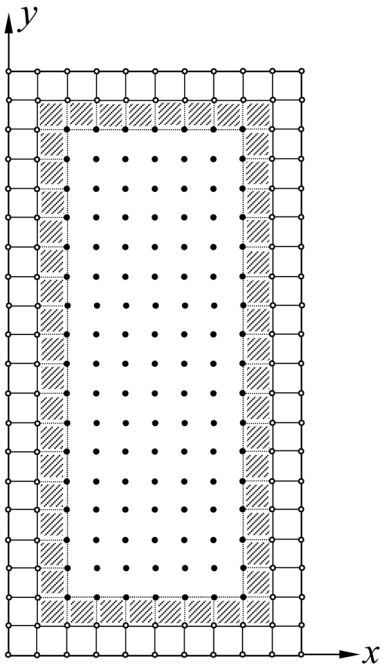

Fig. 13 Regular node arrangement; elements along the four essential boundaries are used to modify the shape functions for example 2

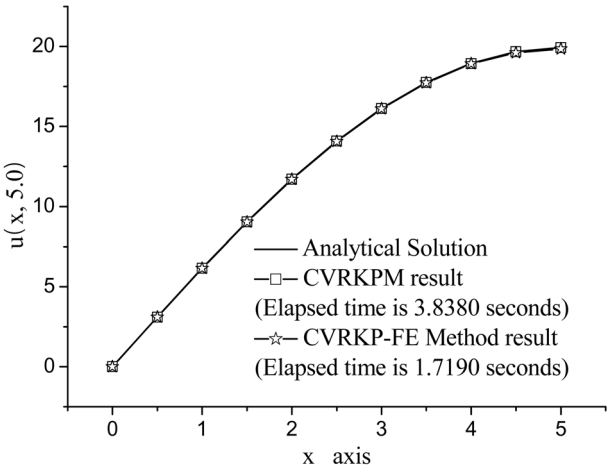

Fig. 14 Temperature distribution along the x axis at $y = 5$

The regular node arrangement when the CVRKPM and CVRKP-FE method are used is shown in Fig. 13. Figs 14 and 15 plot the analytical solution and the numerical solution using the CVRKPM and CVRKP-FE method along the x and y axes, respectively. It is evident that these results are in total agreement with the analytical solution. Moreover, it is again shown that a lesser computational time is needed for the CVRKP-FE method than that of the CVRKPM.

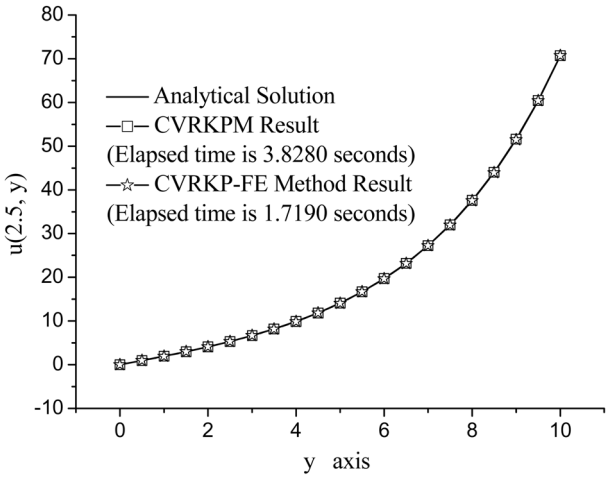

Fig. 15 Temperature distribution along the y axis at $x = 2.5$

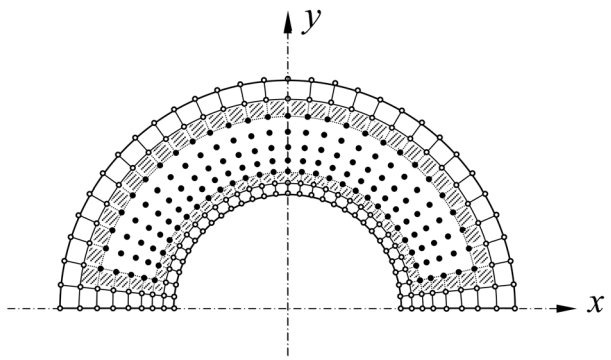

Fig. 16 Nodal arrangement of the coupled CVRKP-FE Method for example 3

5.3 Laplace equation with Dirichlet problems on a half-torus domain

The third example considered is a 2D Laplace equation with Dirichlet boundary conditions, as shown in Fig. 16. The Laplace equation is

$$\nabla^2 u = \frac{\partial^2 u}{\partial x_1^2} + \frac{\partial^2 u}{\partial x_2^2} = 0, \qquad r \in [1, 2], \theta \in [0, \pi] \tag{69}$$

with the boundary conditions

$$u(1, \theta) = \sin(\theta) \qquad 1 < \theta < \pi \tag{70}$$

$$u(2, \theta) = 0 \qquad 1 < \theta < \pi \tag{71}$$

and

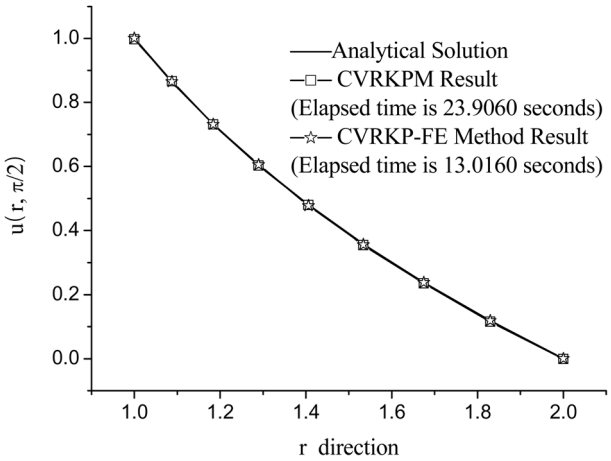

Fig. 17 Values calculated with the analytical, CVRKPM, and CVRKP-FE Method solutions along the r direction where $\theta = \pi / 2$

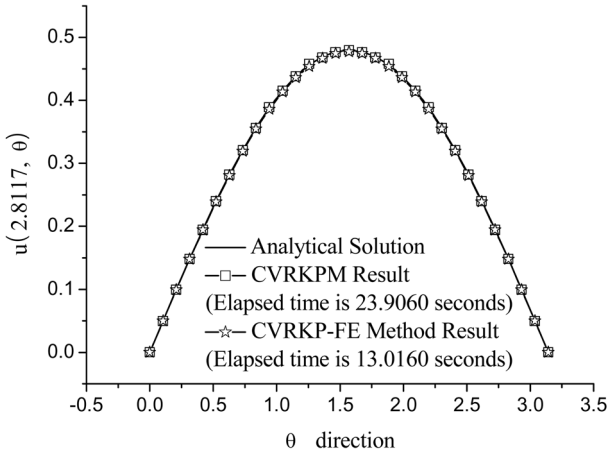

Fig. 18 Compression of the analytical, CVRKPM, and CVRKP-FE Method solutions along the angle axis at $r = 2.8117$

$$u(r, 0) = 0 \qquad 1 < r < 2 \tag{72}$$

$$u(r, \pi) = 0 \qquad 1 < r < 2 \tag{73}$$

The analytical solution of this problem is

$$u(r, \theta) = \frac{3}{4} \times \left[\frac{1}{r} - \frac{r}{4}\right] \times \sin(\theta) \tag{74}$$

The distribution of 279 nodes on a half-torus domain with 9 nodes in the r direction and 31 nodes in the θ direction is considered, as shown in Fig. 16.

Figs 17 and 18 compare the results calculated using the analytical solution, the CVRKPM and the

CVRKP-FE method. The results obtained with the CVRKP-FE method agree well with the analytical solution for the entire domain. Compared with the CVRKPM, the CVRKP-FE method again has high computational efficiency.

6. Conclusions

This paper has discussed the coupling of the complex variable reproducing kernel particle method (CVRKPM) and the finite element method (FEM) for the two-dimensional potential problems. To establish the coupling, interface elements are defined with shape functions composed of the FE and CVRKP shape functions. The discrete equations and corresponding computation formula of the coupled method are then derived. Several numerical example problems are presented to verify the accuracy of the numerical formulations, with the results indicating that the coupled method can effectively reduce the computational cost of the solution with no adverse effect on accuracy. The computational cost is lower because the difficulty of imposing essential boundary conditions for the CVRKPM can be overcome by modeling the portion of the domain with essential boundaries using the FEM, which uses the shape function with the Kronecker delta function property. Hence, the boundary conditions are treated directly, as is usual with the FEM. A comparison of the results of the coupled method and the corresponding analytical solutions demonstrates that the method is both feasible and effective. It should be noted that the proposed method that can also couple other mesh-free methods (Zhang and Liew 2010, Hu *et al*. 2009, Liew *et al*. 2004) with the finite element method.

References

Aluru, N.R. (2000), "A point collocation method based on reproducing kernel approximations", *Comput. Method. Appl. M.*, **47**, 1083-1121.

Atluri, S.N. and Zhu, T.L. (1998), "A new meshless local Petrov-Galerkin (MLPG) approach in computational mechanics", *Computat. Mech.*, **22**, 117-127.

Belytschko, T. and Organ, D. (1995), "Coupled finite element-element-free Galerkin method", *Computat. Mech.*, **17**, 186-195.

Belytschko, T., Krongauz, Y., Organ, D., Fleming, M. and Krysl, P. (1996), "Meshless method: an overview and recent developments", *Comput. Method. Appl. M.*, **139**, 3-47.

Belytschko, T., Lu, Y.Y. and Gu, L. (1994), "Element-free Galerkin methods", *Int. J. Numer. Method. Eng.*, **37**, 229-256.

Chen, J.S., Chen, C., Wu, C.T. and Liu, W.K. (1996), "Reproducing kernel particle methods for large deformation analysis of nonlinear structures", *Comput. Method. Appl. M.*, **139**, 195-229.

Chen, L. and Cheng, Y. (2008a), "Reproducing kernel particle method with complex variables for elasticity", *Acta Physica Sinica*, **57**, 1-10 (in Chinese).

Chen, L. and Cheng, Y. (2008b), "Reproducing kernel particle method with complex variables for transient heat conduction problems", *Acta Physica Sinica*, **57**, 6047-6055 (in Chinese).

Dolbow, J. and Belytschko, T. (1999), "Volumetric locking in the element free Galerkin method", *Int. J. Numer. Meth. Eng.*, **46**, 925-942.

Gu, T.Y. and Liu, G.R. (2005), "Meshless methods coupled with other numerical method", *Tsinghua Sci. Technol.*, **10**, 8-15.

Hu, H.Y., Lai, C.K. and Chen, J.S., (2009), "A study on convergence and complexity of reproducing kernel collocation method", *Interact. Multiscale Mech.*, **2**(3), 295-319.

Kothnur, V.S., Mukherjee, S. and Mukherjee, Y.X. (1999), "Two dimensional linear elasticity by the boundary node method", *Int. J. Solids Struct.*, **36**, 1129-1147.
Liew, K.M. and Chen, X.L. (2004a), "Mesh-free radial basis function method for buckling analysis of non-uniformly loaded arbitrarily shaped shear deformable plates", *Comput. Method. Appl. M.*, **193**, 205-224.
Liew, K.M. and Chen, X.L. (2004b), "Mesh-free radial point interpolation method for the buckling analysis of Mindlin plates subjected to in-plane point loads", *Int. J. Numer. Meth. Eng.*, **60**, 1861-1877.
Liew, K.M. and Cheng, Y. (2009), "Complex variable boundary element-free method for two-dimensional elastodynamic problems", *Comput. Method. Appl. M.*, **198**, 3925-3933.
Liew, K.M. and Huang, Y.Q. (2003), "Bending and buckling of thick symmetric rectangular laminates using the moving least-squares differential quadrature method", *Int. J. Mech. Sci.*, **45**, 95-114.
Liew, K.M., Cheng, Y. and Kitipornchai, S. (2005), "Boundary element-free method (BEFM) for two-dimensional elastodynamic analysis using Laplace transform", *Int. J. Numer. Meth. Eng.*, **64**, 1610-1627.
Liew, K.M., Cheng, Y. and Kitipornchai, S. (2006), "Boundary element-free method (BEFM) and its application to two-dimensional elasticity problems", *Int. J. Numer. Meth. Eng.*, **65**, 1310-1332.
Liew, K.M., Feng, C., Cheng, Y. and Kitipornchai, S. (2007), "Complex variable moving least-squares method: A meshless approximation technique", *Int. J. Numer. Meth. Eng.*, **70**, 46-70.
Liew, K.M., Huang, Y.Q. and Reddy, J.N. (2003), "Moving least-squares differential quadrature method and its application to the analysis of shear deformable plates", *Int. J. Numer. Meth. Eng.*, **56**, 2331-2351.
Liew, K.M., Huang, Y.Q. and Reddy, J.N. (2004), "Analysis of general shaped thin plates by the moving least-squares differential quadrature method", *Finite Elem. Anal. Des.*, **40**, 1453-1474.
Liew, K.M., Huang, Y.Q. and Reddy, J.N. (2004), "Analysis of general shaped thin plates by the moving least-squares differential quadrature method", *Finite Elem. Anal. Des.*, **40**, 1453-74.
Liew, K.M., Ng, T.Y. and Wu, Y.C. (2002a), "Meshfree method for large deformation analysis - a reproducing kernel particle approach", *Eng. Struct.*, **24**, 543-551.
Liew, K.M., Ng, T.Y., Zhao, X. and Reddy, J.N. (2002), "Harmonic reproducing kernel particle method for free vibration analysis of rotating cylindrical shells", *Comput. Method. Appl. M.*, **191**, 4141-4157.
Liew, K.M., Wang, J., Tan, M.J. and Rajendran, S. (2004), "Nonlinear analysis of laminated composite plates using the mesh-free kp-Ritz method based on FSDT", *Comput. Method. Appl. M.*, **193**, 4763-4779.
Liew, K.M., Wu, Y.C., Zou, G.P. and Ng, T.Y. (2002b), "Elasto-plasticity revisited: Numerical analysis via reproducing kernel particle method and parametric quadratic programming", *Int. J. Numer. Meth. Eng.*, **55**, 669-683.
Liu, W.K. and Chen, Y.J. (1995), "Wavelet and multiple scale reproducing kernel methods", *Int. J. Numer. Meth. Fl.*, **21**, 901-931.
Liu, W.K. and Jun, S. (1998), "Multiple-scale reproducing kernel particle methods for large deformation problems", *Int. J. Numer. Meth. Eng.*, **41**, 1339-1362.
Liu, W.K., Chen, Y., Jun, S., Chen, J.S. and Belytschko, T. (1996), "Overview and applications of the reproducing kernel particle methods", *Archives of Computer Methods in Engineering*, State of the Art Review **3**, 3-80.
Liu, W.K., Jun, S. and Zhang, Y.F. (1995), "Reproducing kernel particle methods", *Int. J. Numer. Meth. Fl.*, **20**, 1081-1106.
Liu, W.K., Jun, S., Li, S., Adee, J. and Belytschko, T. (1995), "Reproducing kernel particle methods for structural dynamics", *Int. J. Numer. Meth. Eng.*, **38**, 1655-1679.
Liu, W.K., Jun, S., Thomas, S.D., Chen, Y. and Hao, W. (1997), "Multiresolution reproducing kernel particle method for computational fluid mechanics", *Int. J. Numer. Meth. Fl.*, **24**, 1391-1415.
Liu, Y., Liew, K.M., Hon, Y.C. and Zhang, X. (2005), "Numerical simulation and analysis of an electroactuated beam using a radial basis function", *Smart Mater. Struct.*, **14**, 1163-1171.
Onarte, E. (1996), "A finite point method in computational mechanics", *Int. J. Numer. Meth. Eng.*, **39**, 3839-3866.
Selvadurai, A.P.S. (2000) *Partial differential equations in mechanics 1*, Berlin, Heidelberg: Springer.
Sun, Y.Z., Zhang, Z., Kitipornchai, S. and Liew, K.M. (2006), "Analyzing the interaction between collinear interfacial cracks by an efficient boundary element-free method", *Int. J. Eng. Sci.*, **44**, 37-48.
Zhang, Z. and Liew, K.M. (2010), "Improved element-free Galerkin method (IEFG) for solving three-

dimensional elasticity problems", *Interact. Multiscale Mech.*, **3**, 123-143.
Zhao, X., Ng, T.Y. and Liew, K.M. (2004), "Free vibration of two-side simply-supported laminated cylindrical panels via the mesh-free kp-Ritz method", *Int. J. Mech. Sci.*, **46**, 123-142.
Zhao, X., Yang, Y. and Liew, K.M. (2007), "Geometrically nonlinear analysis of cylindrical shells using the element-free kp-Ritz method", *Eng. Anal. Bound. Elem.*, **31**, 783-792.
Zhu, T., Zhang, J.D. and Atluri, S.N. (1998), "A local boundary integral equation (LBIE) method in computational mechanics and a meshless discretization approach", *Computat. Mech.*, **21**, 223-235.